Strangeness production in proton and heavy ion collisions at 200A GeV

N. S. Amelin
Institut für Theoretische Physik, Universität Frankfurt, D-6000 Frankfurt am Main 11, Germany

L. V. Bravina and L. P. Csernai
Centre for Theoretical Physics, Physics Department, University of Bergen, Allègaten 55, N-5007 Bergen, Norway

V. D. Toneev and K. K. Gudima
Joint Institute for Nuclear Research, Laboratory of Theoretical Physics, Dubna, Russia

S. Yu. Sivoklokov
Institute of Nuclear Physics, Moscow State University, 119899 Moscow, Russia
(Received 19 November 1992)

Strangeness production at the CERN Super Proton Synchroton energies is studied within the quark-gluon string model. The observed shape of rapidity and transverse mass distributions are reproduced fairly well for both peripheral and central heavy ion collisions. However, for central collisions the model underpredicts strange particle abundances by a factor of about 2:2:4 for K^0_S, Λ, and $\bar{\Lambda}$, respectively. This discrepancy can be considered as a possible manifestation of collective string-string interactions similar to the formation of a color rope. Model predictions for coming experiments with the Pb beam at CERN are given.

PACS number(s): 25.75.+r, 24.85.+p, 25.40.−h, 25.40.Ve

I. INTRODUCTION

Heavy ion experiments at ultrarelativistic energies have largely been motivated by the search for a quark-gluon plasma (QGP), a macroscopic state of matter where quarks and gluons are free to move in a large volume. Enhanced strangeness production [1, 2] in ultrarelativistic heavy ion collisions is one of the most widely discussed signatures for creating QGP. Various models were developed to study this signature in different dynamical scenarios. Recently, several experiments have been performed to investigate strangeness production in reactions involving relativistic nuclei, particularly NA35 and WA85 at the CERN Super Proton Synchrotron (SPS), and E802, E810, and E814 at the Brookhaven National Laboratory Alternating Gradient Synchrotron (BNL AGS). The predictions of the quark-gluon string model (QGSM) for AGS energies were presented in Ref. [3]. Most of the results show an increased strangeness production above the $p+p$ data, and sometimes even above previous theoretical expectations. An exciting finding of the last experiments with the 200A GeV Sulphur beam at CERN SPS is the observation of an increase in abundance for strange particles and antiparticles when one proceeds from peripheral collisions to central ones [4–6]. This effect has not been observed at the lower AGS BNL energies of about 15A GeV [7] or at the CERN SPS energy of 200A GeV for lighter projectiles [8]. As has been discussed in a previous work [3], the E802 measurements at the AGS BNL can be understood within the quark-gluon string model (QGSM).

In this article, we present rapidity and transverse momentum distributions of protons, negative and neutral strange particles in p+S and S+S collisions at 200A GeV and compare our calculations with NA35 [4,5] and WA85 [6] SPS CERN experiments. We present also the mean multiplicities of the above particles in the acceptance of NA35 and in the full rapidity range as predicted by the QGSM for p+S, S+S, and central Pb+Pb collisions at the energy of 200A GeV.

Before passing to the calculational results, one should note that the QGSM includes neither the formation of QGP nor some collective dynamics on either the hadronic or string level. Had a noticeable discrepancy between experiment and QGSM predictions been observed, both possibilities should be considered in order to obtain a complete assessment of the strangeness production problem.

II. THE MONTE CARLO QUARK-GLUON STRING MODEL

The QGSM is a detailed realistic microscopic model [9–11] based on string phenomenology of hadronic interactions. In the case of hadron-hadron ($h+h$), hadron-nucleus ($h+A$), and nucleus-nucleus ($A+A$) collisions, one or more strings can be formed which decay later into secondary hadrons. The QGSM takes into account that the string decay products (stable hadrons and their excited states resonances) can interact again with other hadrons. Yet one new physics feature is included in the model: the interaction of strings (treated in an approximate way by allowing the diquarks in a string, which have not yet been hadronized, to rescatter). However, string fragmentation into hadrons occurs independently like in free hadron collisions. There are other models

which also include similar features like the relativistic quantum molecular dynamics (RQMD) by Sorge and coworkers [12–14] and the last version of VENUS by Werner [15].

The QGSM has several possibilities to account for production of strange particles and their transverse momentum distributions. The strange production rate is determined by the strange quark content of the colliding hadrons and by the strangeness suppression probability at string breakup. Strange hadrons are created by the decay of strings with strange and nonstrange quarks at their ends. In the QGSM the model parameters that influence most strangeness abundance are the flavor formation probabilities and the probabilities of the quark-pair, diquark-pair formation at string breaking.

Two- and three-particle reactions, which are not going through string formation, are important for strangeness production and absorption also (see Ref. [3]).

The transverse motion of hadrons in the QGSM arises from different sources: primordial transverse momentum of the constituent quarks, transverse momentum of both quark-antiquark and diquark-antidiquark pairs acquired at string breakup, the original transverse Fermi motion of nucleons in projectile and target, and finally rescatterings of secondaries or of leading valence quarks or diquarks of a string which are not yet completely hadronized. Parameters of the first two sources are fixed by hadronic data. The Fermi motion changes the effective transverse distribution of strings formed by the valence quarks and diquarks of the initial projectile and target nucleons. Hence, the original strings formed by the valence quarks or diquarks of the initial projectile and target nucleons are not completely parallel to the beam axis. The last source is a purely nuclear one and can result in some observable effects. For example, considerable transverse momentum arising due to secondary interactions may give rise to some azimuthal asymmetry, the so-called transverse flow, as was pointed out in an earlier publication [16].

The parameters of the model were adjusted to the known $h + h$ and $h + A$ data.

III. CENTRAL S+S EVENTS. NONSTRANGE PARTICLE PRODUCTION

The QGSM provides a tool to predict rapidity, y, and $p_\perp$ distributions for produced hadrons. Comparing transverse momentum distributions for different hadrons is convenient to do in terms of transverse mass, $m_T = \sqrt{{p_\perp}^2 + {m_0}^2}$ shifted by the value of a hadron mass m_0, that is $m_T - m_0$, called *transverse kinetic energy*. In this paper we use this variable.

As has been shown in previous works [9, 17], proton and pion rapidity distributions and $p_\perp$ spectra measured at SPS CERN are well reproduced by the QGSM for ^{16}O-induced reactions. This turns out to be true also for central S+S collision data [4, 5, 18] (see Figs. 1 and 2), and means that our model describes correctly the overall evolution of a colliding system. Note that some kind of thermalization is approached even for the baryonic component as follows from noticeable enhancement of the proton yield at midrapidities. The latter results from string-string scatterings and secondary interactions particles arising from earlier string hadronization. This takes place even far behind the nucleus due to finiteness of the hadron formation time. It is of interest that the widely discussed [19] two-component structure of the transverse momentum spectrum of pions is nicely fitted by the QGSM. Note that the production and decay of

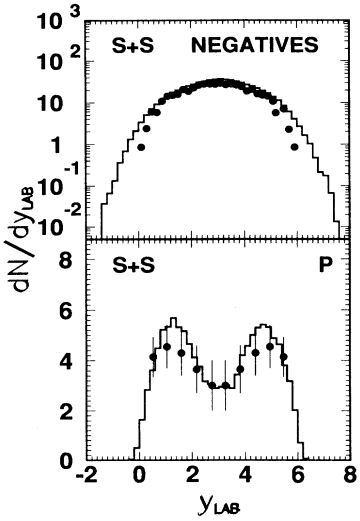

FIG. 1. Rapidity distribution of protons and negative particles from central S+S collisions at the energy of 200A GeV. Circles are experimental points of the NA35 Collaboration [4, 5, 18]. Histograms are QGSM results.

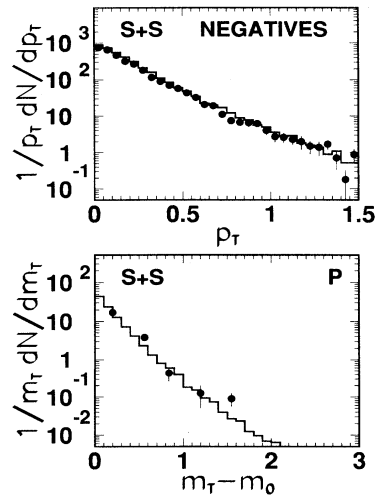

FIG. 2. Transverse momentum, p_T (in GeV/c), distribution of negatives and transverse kinetic energy, $m_T - m_0$ [GeV/c^2], distribution of protons from central S+S collisions at energy 200A GeV. The rapidity acceptance intervals are $0.8 < y < 2.0$ for negative hadrons and $1.5 < y < 2.7$ for protons. Notation is the same as in Fig. 1.

hadronic resonances (mostly Δ's) contributing to the low $p_\perp$ region are taken into account properly.

IV. NEUTRAL STRANGE PARTICLE PRODUCTION

A. p+S collisions

It is quite instructive to start the consideration of strangeness production from the p+S collisions to see how well the QGSM works for this simple case in the NA35 acceptance. As follows from Figs. 3 and 4 the shape of rapidity and transverse mass spectra for kaons, lambdas, and anti-lambdas is reproduced fairly well. The rapidity spectra of newly produced hadrons (K^0_S and $\bar{\Lambda}$) have a sharp peak in the midrapidity range. The model agrees with this observation. The target-fragmentation region dominates in the rapidity distribution of lambdas, so that the Λ yield in the central region of rapidity spectra is underestimated by the QGSM. The model fits the slopes of transverse mass distributions in the whole kinematic region considered.

For the hadron-nucleus case, the QGSM describes successfully not only the shape of distributions but the absolute yield of strange particles, as well. This is demonstrated by calculational results in Table I, where the average multiplicities of strange particles and accompanying negative hadrons $\langle h^- \rangle^a$ in the NA35 acceptance a are given and compared to the data [4, 5, 18]. For completeness, data for $p + p$ collisions are included, as well. Average hadron multiplicities in the whole phase space $\langle h \rangle$ are even in a better agreement with the data.

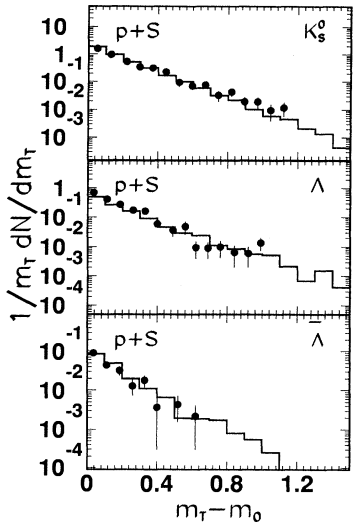

FIG. 4. Transverse kinetic energy distributions for neutral strange particles produced in p+S collisions at 200A GeV. Events with $h_{\rm ch} > 5$ are selected. The rapidity acceptance intervals are $0.8 < y < 4.2$ for Λ, $1.7 < y < 4.2$ for K^0_S, and $0.8 < y < 4.2$ for $\bar{\Lambda}$. Notation is the same as in Fig. 1.

B. S+S collisions

The rapidity and transverse mass distributions for strange particles produced in the central S+S collisions are presented in Figs. 5 and 6. The total number of events generated with impact parameter $b = 0$ fm is 1500. In the calculation the experimental acceptance for mea-

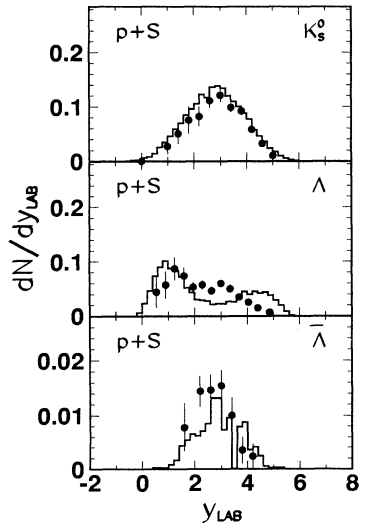

FIG. 3. Rapidity distribution for neutral strange particles produced in p+S collisions at 200 GeV. Events with charged hadron multiplicity, $h_{\rm ch} > 5$, are selected. The rapidity distributions correspond to the full transverse momentum range. Notation is the same as in Fig. 1.

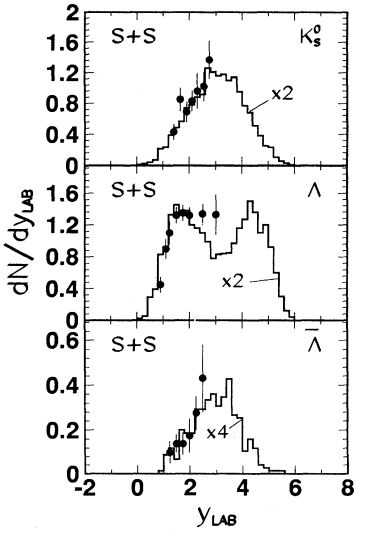

FIG. 5. Rapidity distributions of K^0_S, Λ, and $\bar{\Lambda}$ per trigger in central S+S collisions at the energy of 200A GeV. The rapidity distributions are for transverse momentum, $p_T > 0.5$ GeV/c (0.62 GeV/c) for Λ, $\bar{\Lambda}$ (K^0_S), respectively. Theoretical QGSM values are multiplied by the factors shown in the figure. Notation is the same as in Fig. 1.

TABLE I. Comparison of neutral strange particle multiplicities observed in the NA35 acceptances with the QGSM predictions. Data are given for p+S (minimum bias, excluding events with charged hadron multiplicity $h_{\rm ch} \leq 5$) and p+p collisions (extracted by the NA35 Collaboration from different measurements, see [4, 5, 18]). Total negative hadron multiplicities, $\langle h^- \rangle$, and associated multiplicities, $\langle h^- \rangle^{a,b}$, representing the fraction of $\langle h^- \rangle$ that falls into the acceptance region of (a) K^0_S and (b) Λ and $\bar{\Lambda}$ of the NA35 experiment are also given for the reactions considered.

Reaction (selected events)	NA35 $p+p$	QGSM $p+p$	NA35 p+S ($h_{\rm ch} > 5$)	QGSM p+S ($h_{\rm ch} > 5$)
$\langle h^- \rangle$	2.850 ± 0.040	2.790	5.50 ± 0.20	5.520
$\langle K^0_S \rangle^a$	0.022 ± 0.004	0.029	0.06 ± 0.01	0.057
$\langle h^- \rangle^a$			0.39 ± 0.03	0.51
$\langle \Lambda \rangle^b$	0.0190 ± 0.0060	0.0320	0.070 ± 0.010	0.080
$\langle \bar{\Lambda} \rangle^b$	0.0014 ± 0.0006	0.0028	0.006 ± 0.002	0.0044
$\langle h^- \rangle^b$			0.480 ± 0.040	0.56

sured neutral strange particles as well as for accompanying charged hadrons was taken into account accurately.

Similarly to p+S (or peripheral S+S) collisions, the rapidity spectra of K^0_S and $\bar{\Lambda}$ particles have a sharp peak centered at midrapidity, and their widths are close to the ones for the proton-induced case. For Λ particles the distribution is naturally symmetrical and its width is larger due to possible production of strange baryons in the target (projectile) fragmentation region. It is interesting to note that the calculated rapidity spectrum for lambdas from central S+S collisions exhibits a distinct dip at midrapidities like in the proton distribution while the experiment shows a quite flat behavior at these rapidities. However, statistical uncertainties for this rapidity range are large enough in the NA35 experiment; this point is quite important for estimating the total multiplicity of lambdas.

According to the NA35 data the effective temperatures for Λ, $\bar{\Lambda}$, and K^0 are around $T = 193 - 194$ MeV in S+S collisions, compared to $T_\Lambda = 174$ MeV and $T_{K^0} = 206$ MeV in p+S collisions. As seen from Fig. 6 the QGSM gives a perfect description of the slope of transverse kinetic energy distribution for all strange particles considered.

An important experimental observation of the WA85 Collaboration (particles measured with $p_t \geq 1$ GeV/c) is that the Λ and $\bar{\Lambda}$ effective temperatures (or slope parameters) are rather high, $T \approx 230$ MeV, at the energy of 200A GeV for S+W collisions. The slope parameter of negative hadrons is even higher, $T \approx 250$ MeV [6]. These slopes are reproduced by QGSM. It is an interesting consequence that particles containing valence diquarks have a larger transverse momentum than particles containing an antiquark-diquark pair because in the QGSM they have a contribution from the original Fermi motion, too. In particular, this leads to a higher effective temperature for Λ's than for $\bar{\Lambda}$'s [6].

This success of the QGSM is related to taking into consideration the nonequilibrium nature of an interacting string-hadron system and all subsequent interactions of system constituents. The equilibrium thermodynamic consideration using the initial temperature as a free parameter fails to reproduce simultaneously the shape of transverse mass distributions for all hadrons even if resonance decays would be included [19].

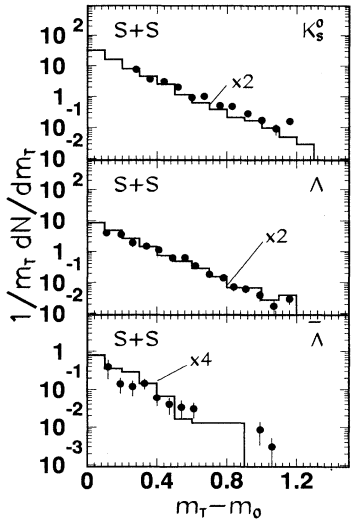

FIG. 6. Transverse kinetic energy distributions of K^0_S, Λ, and $\bar{\Lambda}$ in central S+S collisions at the energy of 200A GeV. The rapidity acceptance intervals are $0.8 < y < 2.0$ for Λ, $1.5 < y < 2.7$ for K^0_S, and $0.8 < y < 2.0$ for $\bar{\Lambda}$. Theoretical QGSM values are multiplied by the factors shown in the figure. Notation is the same as in Fig. 1.

C. Strange particle abundance in central S+S collisions

Although the existing trends of hadron distributions are quite satisfactorily approximated by the quark-gluon string model, this approximation is getting less reliable for strange particle abundances produced in heavy colliding systems. In our case, this is evidently seen in the model results for central S+S collisions. The needed multiplication factors to match the experimental data are shown in Figs. 5 and 6, and the average hadron multi-

TABLE II. Comparison of neutral strange particle multiplicities observed in the NA35 acceptances with the QGSM predictions. Data for S+S collisions (3 trigger modes) and predictions for Pb+Pb collisions are given. The total negative hadron multiplicities, $\langle h^- \rangle$, and associated multiplicities, $\langle h^- \rangle^{a,b}$, representing the fraction of $\langle h^- \rangle$ that falls into the acceptance regions of (a) K^0_S and (b) Λ and $\bar{\Lambda}$ of the NA35 experiment are also given for the reactions considered.

Reaction (trigger modes)	$\langle h^- \rangle$	$\langle K^0_S \rangle^a$ $\langle h^- \rangle^a$	$\langle \Lambda \rangle^b$ $\langle h^- \rangle^b$	$\langle \bar{\Lambda} \rangle^b$ $\langle h^- \rangle^b$
NA35 S+S	18.5 ± 1.5	0.20 ± 0.04	0.29 ± 0.06	-
$(10 < h_{\rm ch} < 100)$	-	1.33 ± 0.10	1.67 ± 0.13	-
QGSM S+S	18.5	0.17	0.24	0.011
$(10 < h_{\rm ch} < 100)$	-	1.25	1.46	1.460
NA35 S+S	70.0 ± 4.0	1.27 ± 0.40	1.28 ± 0.35	-
$(h_{\rm ch} > 100)$	-	5.00 ± 0.25	5.91 ± 0.30	-
QGSM S+S	78.0	0.65	0.77	0.041
$(h_{\rm ch} > 100)$	-	5.05	5.59	5.590
NA35 S+S	103 ± 5	1.85 ± 0.11	2.30 ± 0.12	0.31 ± 0.05
(central)	-	7.90 ± 0.25	9.40 ± 0.30	9.40 ± 0.30
QGSM S+S	118	0.94	1.25	0.085
($b = 0$ fm)	-	7.43	8.18	8.18
QGSM Pb+Pb	1512	7.5	9.1	0.47
($b = 0$ fm)	-	54.9	63.0	63.0

plicities for different triggers (i.e., different impact parameter selection) are compared with experimental data in Table II. In the most central 200A GeV S+S collisions, the Λ and K abundance is underpredicted by a factor of about 2; and $\bar{\Lambda}$ abundance, by a factor of 4.

From Table III one can find the $\langle h^- \rangle$ dependence of the experimental ratios, extrapolated to the full phase space, and model ratios of strange particle multiplicity to the total multiplicity of negatively charged particles which are mainly pions. Roughly, this ratio is proportional to the relative content of strange quark-antiquark pairs, $\bar{s}s/(\bar{u}u + \bar{d}d)$. The NA35 experimental ratios $\langle K^0_S \rangle / \langle h^- \rangle$ and $\langle \Lambda \rangle / \langle h^- \rangle$ were found to increase by a factor of about 2, going from $p + p$ to central S+S collisions and by a factor of about 3 for the ratio $\langle \bar{\Lambda} \rangle / \langle h^- \rangle$.

In the string model FRITIOF [20], which is neglecting secondary interactions, these ratios should be equal to that for nucleon-nucleon collisions because the strings produced in nucleon-nucleon and nucleus-nucleus collisions have the same valence quark content as the initial nucleons, and particle ratios are governed by the same strangeness and antibaryon suppression parameters. This is also true for the QGSM and RQMD [12–14] approaches if secondary rescatterings are switched off.

In the QGSM approach, secondary interactions at energies lower than the threshold for strange particle production lead even to decreasing ratios (by a factor of about 2 for Pb+Pb collisions) while experimental ratios have an opposite trend: Strangeness abundance grows with increasing negative multiplicity (decreasing impact parameter). The most drastic difference is observed for the $\bar{\Lambda}$ production.

It should be noted that in the QGSM the relative abundance of strange baryons and antibaryons (Λ and $\bar{\Lambda}$) versus negatives is reproduced for p+W [6] but the QGSM underpredicts the Λ and $\bar{\Lambda}$ yields measured by the WA85

TABLE III. Comparison of experimental multiplicities of negative hadrons and neutral strange particles, extrapolated to full phase space (upper lines), in $p + p$, p+S, and central S+S collisions with QGSM predictions (lower lines).

Reaction	$\langle h^- \rangle$	$\langle K^0_S \rangle$	$\langle \Lambda \rangle$	$\langle \bar{\Lambda} \rangle$
NA35 p+p	2.85 ± 0.04	0.17 ± 0.01	0.095 ± 0.010	0.013 ± 0.004
QGSM p+p	2.85	0.21	0.15	0.015
NA35 p+S	5.00 ± 0.2	0.28 ± 0.03	0.22 ± 0.02	0.028 ± 0.004
QGSM p+S	5.87	0.34	0.24	0.023
NA35 S+S	103 ± 5	10.7 ± 2.0	8.2 ± 0.9	1.50 ± 0.4
QGSM S+S	120	7.4	4.7	0.35
QGSM Pb+Pb	1536	93.4	49.6	1.73

Collaboration [21]. At the same time the slopes of the $p_\perp$ spectra are reproduced.

In VENUS [15], in the multichain model by Ranft [22] or in the version of the QGSM [17] which belongs to the so-called dual parton approach, the ratios considered above can be rather different from that for nucleon-nucleon collisions because newly produced strings can have not only a valence, but also a sea quark at their ends. The number of strings having a sea quark depends on the number of nucleon interactions, i.e., from the centrality of nucleus-nucleus collisions. The model strangeness abundance is governed also by the strange sea-quark structure of a nucleon. In Ref. [23], it was shown that the proper choice of the amount of strange sea-quark component of nucleon structure function gives a possible explanation of the abundance of the neutral kaons in central S+S collisions.

V. MODEL PREDICTIONS FOR Pb+Pb COLLISIONS

It is of great interest to look at what predictions are given by the QGSM for the heaviest colliding systems. Such results for central Pb+Pb collisions at the energy of 200A GeV and for acceptance of the NA35 experiment are presented in Table II, and in Figs. 7 and 8, where data for central S+S collisions are shown for comparison also. The following remarks should be made about these results:

A huge number of hadrons is produced in lead-on-lead collisions. Specific numbers depend essentially on selected windows in the rapidity and transverse momentum phase space. As to the mass-dependence of total multiplicity, the two available experimental points may be well approximated by $\langle h^- \rangle \sim A^{4/3}$. The average abundance of strange particles is $\langle K_S^0 \rangle : \langle \Lambda \rangle : \langle \bar{\Lambda} \rangle = 93:50:1.7$; thus, strange particle interferometry measurements on an event-by-event basis become feasible.

The baryonic rapidity spectra are tending to a "bell-like" shape; thus lots of baryons will be at midrapidities (Fig. 7). This effect has been noted for protons in Ref. [24]. In the present QGSM calculation we have found the same for Λ particles also (Fig. 9).

As seen in Fig. 7 the negative hadron density in the

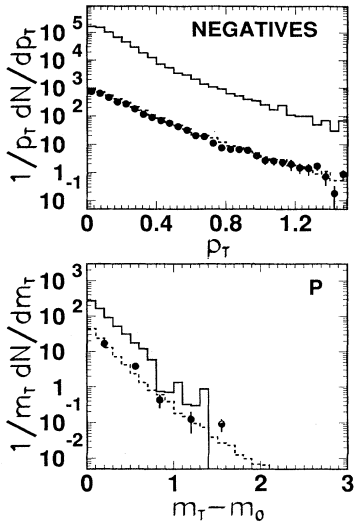

FIG. 8. Predicted transverse momentum distributions of negatives and transverse kinetic energy distributions of protons in central Pb+Pb (full lines) and S+S (dashed lines) collisions at 200A GeV. The rapidity acceptance intervals are $0.8 < y < 2.0$ for negative hadrons and $0.8 < y < 2.0$ for protons. Notation is the same as in Fig. 1.

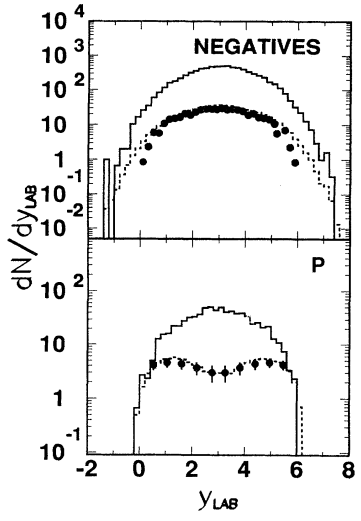

FIG. 7. Predicted rapidity distributions of negatives and protons per trigger in central Pb+Pb (full lines) and S+S (dashed lines) collisions at the energy of 200A GeV. Notation is the same as in Fig. 1.

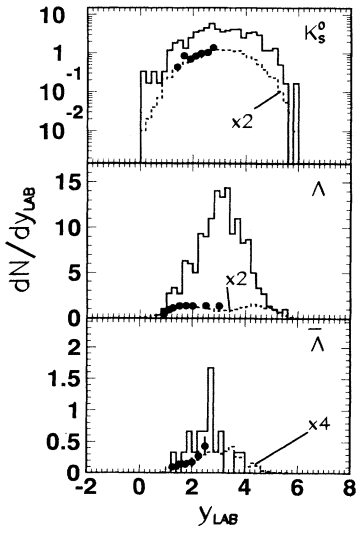

FIG. 9. Rapidity distributions of K_S^0's, Λ's, and $\bar{\Lambda}$'s per trigger in central Pb+Pb (full lines) and S+S (dashed lines) collisions at the energy of 200A GeV. Notation is the same as in Fig. 1.

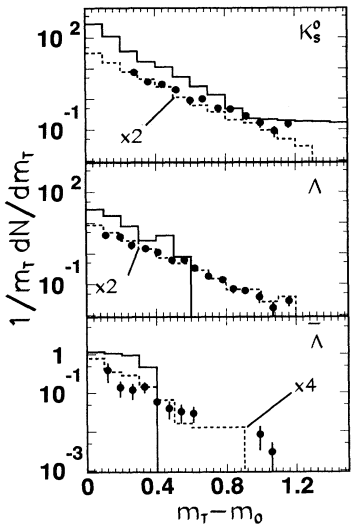

FIG. 10. Transverse kinetic energy distributions of K_S^0's, Λ's, and $\bar{\Lambda}$'s in central Pb+Pb (full lines) and S+S (dashed lines) collisions at 200A GeV. The rapidity acceptance intervals are the same as in Fig. 6. Notation is the same as in Fig. 1.

midrapidity range is expected to be about 500. Using the simple formula [25], we get for the energy density $\epsilon \approx 10\ \mathrm{GeV/fm^3}$ if $\tau_0 = 1$ fm. This value is higher than the maximal transverse energy density resulting from the dynamical consideration of evolution of the colliding system [17]. This observation is not very surprising because the QGSM dynamics differs quite essentially from the Bjorken dynamics which assumes free stemming of baryonless matter.

The transverse mass spectra of negatives look similar for both combinations of colliding nuclei, but the two-slope structure of distributions seems to be more noticeable in the Pb+Pb case (Fig. 8). The slope parameter of the proton transverse mass distribution is approximately the same for S+S and Pb+Pb collisions. However, spectra of strange particles, e.g., K_s^0, are softened going from S+S to Pb+Pb (Fig. 10). This effect is due to the fact that strange hadrons are produced mainly in secondary interactions.

VI. DISCUSSION AND CONCLUSIONS

As has been shown above and in previous works [3, 9, 17], the quark-gluon string model is quite successful in describing a large variety of characteristics of hadron– and heavy-ion–induced reactions in both BNL-AGS and CERN-SPS energy regions. A quantitative prediction is given for the rapidity and transverse kinetic energy distribution of neutral strange particles in p+S collisions at 200 GeV, except the rapidity distribution of Λ. The QGSM gives a quantitative prediction of rapidity and transverse momentum distribution of pions and protons in central S+S at 200A GeV. Furthermore, the model reproduces the observed enhancement of the low-$p_\perp$ spectrum for negatively charged particles measured by the NA35 Collaboration. The QGSM describes correctly the shapes of the rapidity and transverse kinetic energy distributions in central S+S at 200A GeV collisions for neutral strange particles.

The most striking discrepancy is found for the strange particle abundance in central S+S collisions at the energy of 200A GeV. In this connection the NA35 data are in an exceptional position because a strangeness enhancement with decreasing impact parameter has not been observed at lower AGS-BNL energies [7] or for the same energy 200A GeV with lighter projectile [8]. Such a large excess of strangeness can signal a possible transition (or proximity) of an excited hadronic matter into quark-gluon phase or some essential change in the interaction dynamics.

Dynamical consideration of the energy density evolution for central S+S collisions shows [17] that on the average a system spends less than 0.5 fm/c in the state with average transverse energy density $\langle \epsilon_t \rangle \geq \epsilon_{\mathrm{cr}} \approx 3$ GeV/fm^3. This short time is not enough for a quark-gluon phase transition to be realized. For central ^{16}O+Au collisions this condition is even worse: $\langle \epsilon_t \rangle \leq \epsilon_{\mathrm{cr}}$ and a critical state can be approached only due to fluctuations [17], if ever.

However, the high energy density means that the density of strings formed in an interaction is high, and an approximation of the independence of strings and of string fragmentation becomes poor. In other words, one should take into account the influence of surrounding strings on the hadronization process of a given string. (A noticeable discrepancy in strange particle abundance between string model predictions and NA35 data and its possible relation to a collective string-string interaction have been mentioned in Refs. [17, 26].) This can be done via different assumptions [27, 28]. The essence of such modifications or improvements of string models are that instead of the usual (triplet) strings fewer but more energetic objects, *double strings* or *fused strings*, are created which enable an easier baryon and strange particle formation.

For a qualitative estimate of the physical consequences of such a collective string-string interaction, we present here some preliminary results of the Monte Carlo string fusion model (SFM) [29] which is based on a simple probabilistic model of string fusion [30]. In this approach it is assumed that strings fuse as soon as partons, which serve as their sources, have their transverse positions close enough. The parton-parton cross section parameter, σ, determines the interaction probability. To describe $\bar{\Lambda}$ enhancement we choose $\sigma = 3.5$ mb [29]. The fused strings possess all energy and momentum of their constituent strings.

The fusion of at most two strings is taken into account, with no more than four valence quarks at the end of a fused string, resulting in color sextet- or octet-fused strings. The string tension for a sextet or octet string is 2.5 times as large as for ordinary (triplet) strings.

Figure 11 demonstrates the $\bar{\Lambda}$ production enhancement as a result of string fusion for different combinations of colliding nuclei at 200A GeV. Without string fusion SFM yields approximately the same rapidity distribution for $\bar{\Lambda}$'s as QGSM. The inclusion of string fusion in

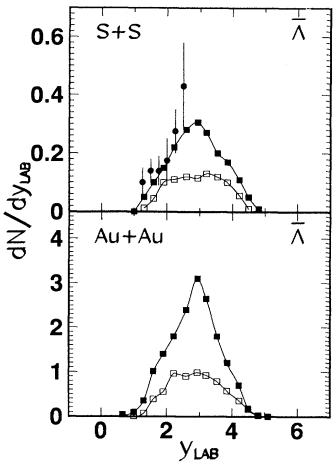

FIG. 11. Rapidity distributions of $\bar{\Lambda}$ per trigger in central S+S and Au+Au collisions at 200A GeV. The rapidity distributions are for transverse momentum, $p_T > 0.5$ GeV/c for $\bar{\Lambda}$. Black circles are experimental data of the NA35 Collaboration [4, 5, 18]. Black and open squares are SFM predictions with and without string fusion respectively.

SFM increases the strange hadron abundances; however, it is not able to describe the experimentally observed strangeness abundances completely. String fusion in the case of Au+Au leads to a somewhat stronger $\bar{\Lambda}$ enhancement than in S+S (Fig. 11). The obtained enhancement of Λ's is not sufficient to explain NA35 data. Thus one has to attach some extra mechanism to describe the data, as was done in Ref. [28]. Moreover, as follows from the above-mentioned calculation [29], string fusion leads to a suppression of total particle production. As a result of competition between strangeness enhancement and particle multiplicity suppression, string fusion does not affect the K_0^S production in the case of central S+S collisions.

Summarizing, one can conclude that the strangeness enhancement observed in central S+S collisions may be considered as a manifestation of a collective string-string interaction, such as formation of a color rope. On the other hand, other possible explanations are not excluded. One may also view fused energetic strings as precursors to a thermalized plasma.

The model predictions presented above for central Pb+Pb collisions give an idea for particle abundances in experiments planned in the near future at CERN and, at the same time, can serve as a test of the hypothesis of a color rope formation. We believe that our predictions for nonstrange hadrons will turn out to be close to what will be measured, but we expect that strange particle abundances are underpredicted by the model. This difference, being compared to the S+S case, can shed additional light on the origin of strangeness production. The shape of transverse mass spectra of strange and nonstrange hadrons is also of great interest.

ACKNOWLEDGMENTS

We are grateful to H.-W. Barz, M. Braun, B. Friman, J. Knoll, P. Levai, C. Pajares, and H. Schulz for useful discussions and especially to H. Ströbele for elucidating the experimental cut problem in the NA35 experiment. Valuable contributions of E. F. Staubo are gratefully acknowledged. This work was supported by the Norwegian Research Council for Science and Humanities and the General Direction of the Scientific and Technical Investigation of Spain. N.S.A. acknowledges the financial support of the Alexander von Humboldt Foundation. L.P.C. acknowledges support from NATO under grant CRG. 920322-644.

[1] J. Rafelski and B. Müller, Phys. Rev. Lett. **48**, 1066 (1982); **56**, 2334(E) (1986).
[2] P. Koch, B. Müller, and J. Rafelski, Phys. Rep. **142**, 169 (1986).
[3] N.S. Amelin, E.F. Staubo, L.P. Csernai, V.D. Toneev, and K.K. Gudima, Phys. Rev. C **44**, 1541 (1991).
[4] J. Bartke *et al.*, Z. Phys. C **48**, 191 (1990).
[5] R. Stock, *et al.*, Nucl. Phys. **A525**, 221c (1991).
[6] S. Abatzis *et al.*, Phys. Lett. B **270**, 123 (1991).
[7] J. Stachel, Nucl. Phys. **A527**, 167c (1991).
[8] A. Bombarger *et al.*, Z. Phys. C **43**, 25 (1988).
[9] N.S. Amelin, K.K. Gudima, and V.D. Toneev, *The Nuclear Equation of State*, edited by W. Greiner and H. Stöcker, NATO ASI Series A216 (Plenum, New York, 1989), Pt. B, p. 473.
[10] N.S. Amelin, K.K. Gudima, and V.D. Toneev, Yad. Fiz. **51**, 512 (1990) [Sov. J. Nucl. Phys. **51**, 327 (1990)].
[11] N.S. Amelin, K.K. Gudima, S.Yu. Sivoklokov, and V.D. Toneev, Yad. Fiz. **52**, 272 (1990) [Sov. J. Nucl. Phys. **52**, 172 (1990)].
[12] H. Sorge, H. Stöcker, and W. Greiner, Nucl. Phys. **A498**, 567c (1989).
[13] H. Sorge, A. von Keitz, R. Matiello, H. Stöcker, and W. Greiner, Phys. Lett. B **243**, 7 (1990).
[14] A. von Keitz, H. Sorge, H. Stöcker, and W. Greiner, Nucl. Phys. **A527**, 601 (1991).
[15] K. Werner, Phys. Lett. B **219**, 111 (1989); Z. Phys. C **42**, 85 (1989).
[16] N.S. Amelin, E.F. Staubo, L.P. Csernai, V.D. Toneev, K.K. Gudima, and D. Strottman, Phys. Rev. Lett. **67**, 1523 (1991).
[17] V.D. Toneev, N.S. Amelin, K.K. Gudima, and S. Yu. Sivoklokov, Nucl. Phys. **A519**, 463c (1990).
[18] H. Ströbele *et al.*, Nucl. Phys. **A525**, 59c (1991).
[19] J. Sollfrank, P. Koch, and U. Heinz, Z. Phys. C **52**, 593 (1991).
[20] B. Andersson, G. Gustafson, and B. Nilsson-Almquist, Nucl. Phys. **B281**, 289 (1987).
[21] N. S. Amelin, E. S. Staubo, and L. P. Csernai, Nucl. Phys. (Proc. Suppl.) **B24**, 269 (1991).

[22] J. Ranft, Phys. Rev. D **37**, 1842 (1988).
[23] I. Kawrakov and H.-J. Möhring, J. Ranft, Nucl. Phys. **A544**, 471c (1992).
[24] N.S. Amelin, E.F. Staubo, L.P. Csernai, V.D. Toneev, K.K. Gudima, and D. Strottman, Phys. Lett. B **261**, 352 (1991).
[25] J. Bjorken, Phys. Rev. D **27**, 140 (1983).
[26] N.S. Amelin, K.K. Gudima, V.D. Toneev, and S. Yu. Sivoklokov, in Fourth International Conference on Nucleus-Nucleus Collisions, Kanazava, Japan, 1991, Contributed Papers, C-03, edited by H. Toki, I. Tanihata, and H. Kamitsubo (unpublished).
[27] T.S. Biro, H.B. Nilssen, and J. Knoll, Nucl. Phys. **B245**, 449 (1984).
[28] K. Werner, Nucl. Phys. **A544**, 593c (1992).
[29] N.S. Amelin, M.A. Braun, and C. Pajares, in *Proceedings of the 22nd International Symposium on Multiparticle Dynamics*, Santiago de Compostela, Spain, 1992 (World Scientific, Singapore, in press); N.S. Amelin, M. A. Braun, and C. Pajares, submitted to Nucl. Phys. B.
[30] M. A. Braun and C. Pajares, Phys. Lett. B **287**, 154 (1992).